Earth, Planets and Space

FULL PAPER Open Access

Crust and upper mantle electrical structure of the eastern Central Asian Orogenic Belt revealed by the MT line from Zhangwu County to East Ujimqin Banner

Pengfei Zhao[1,2], Cai Liu[1], Yang Liu[1*], You Tian[1], Xiaodong Chen[1] and Yang Cui[1]

Abstract

The Central Asian Orogenic Belt is bounded on the north by the Siberian Craton and on the south by the North China Craton and the Tarim Craton. It is one of the largest Phanerozoic accretionary orogenic belts on Earth. Since the early Paleozoic, its eastern part has experienced the compound orogenesis and mineralization of three major tectonic systems: the closure of the Paleo-Asian Ocean, the closure of the Mongolian–Okhotsk Ocean, and the subduction of the Paleo-Pacific Plate. From Zhangwu County in the south to East-Ujimqin Banner in the north, a 500 km magnetotelluric profile adjacent to Northeast China has been studied. With 100 sites of magnetotelluric data processing and analysis, we apply a two dimensional inversion in TE and TM modes and obtain a resistivity model up to a 100 km depth. We have discovered two high-resistivity anomalies with opposite dip directions in the upper mantle on both sides of the Solonker Suture Zone, which provide an evidence of the bi-directional subduction pattern of the oceanic crust and the position of the closure of the Paleo-Asian Ocean. In addition, the whole study area presents an approximate basin-range coupling relationship. In the northern part of the study area, the low-resistivity anomalies below it have an apparent north-dipping characteristic, which may be related to the asthenosphere upwelling from west to east. In addition, they may be related to the upwelling of mantle materials, and provide sources of ore-forming material for the Baiyinnuoer mining area through post-collision extension. In the central part of the study area, there are several large-scale high-resistivity anomalies below the Baolidao Belt. The different dip directions reveal the experiences of several subductions and collisions. In the southern part of the study area, the Bainaimiao Belt is located between the southern margin of the Songliao Basin and the northern margin of North China Craton. The main resistivity anomalies below are all south-dipping.

Keywords: The Central Asian Orogenic Belt, Magnetotellurics, Electrical structure model, Structure interpretation

*Correspondence: yangliu1979@jlu.edu.cn

[1] College of Geo-Exploration Science and Technology, Jilin University, Changchun 130026, China
Full list of author information is available at the end of the article

Graphical Abstract

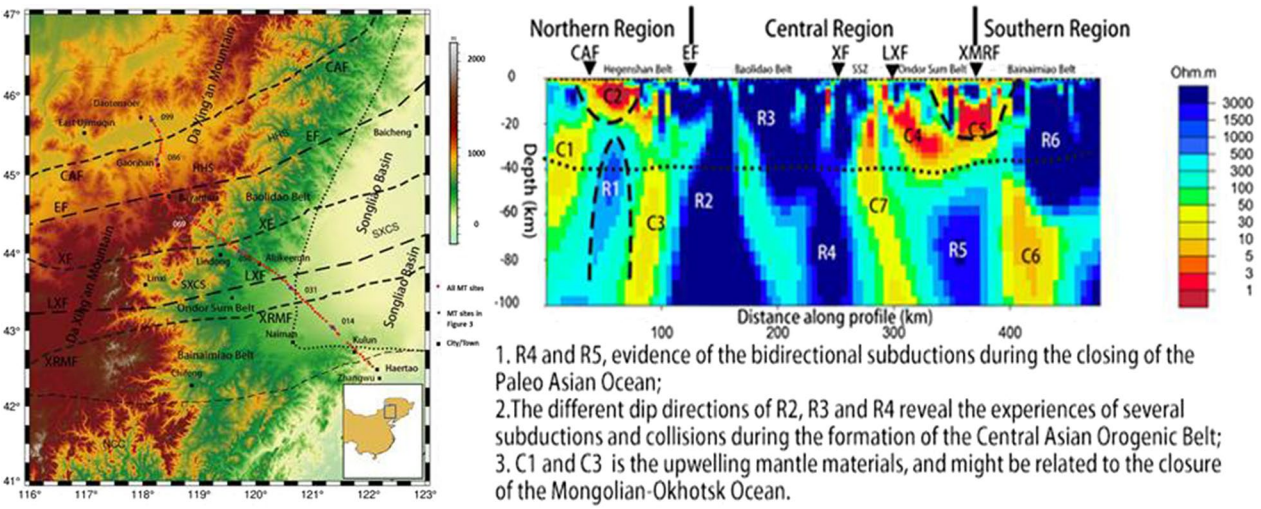

1. R4 and R5, evidence of the bidirectional subductions during the closing of the Paleo Asian Ocean;
2.The different dip directions of R2, R3 and R4 reveal the experiences of several subductions and collisions during the formation of the Central Asian Orogenic Belt;
3. C1 and C3 is the upwelling mantle materials, and might be related to the closure of the Mongolian-Okhotsk Ocean.

Introduction

The Central Asian Orogenic Belt (CAOB), located between the Siberia and North China-Tarim Craton, has been an important area for studying the convergence of multiple plates, because it is one of the largest Phanerozoic accretionary orogenic belts on Earth. Although there is still some controversy about the plate collision events, suture locations, and island arc collapse processes in the region (Shao 1991; Tang et al. 1995; Xiao et al. 2003), scholars generally agree that the eastern part of the CAOB is influenced by three major tectonic systems, including the closure of the Paleo-Asian Ocean and the Mongolian–Okhotsk Ocean and the subduction of the Paleo-Pacific Plate.

The collision and post-collision after the final closure of the Mesozoic Paleo-Asian Ocean, the subduction and closure of the Mongolian–Okhotsk Ocean and its post-collisional extensional orogeny, and the subduction of the Paleo-Pacific Plate provide necessary geological background for the study of the tectonic framework and mineralization mechanisms in the Far East, including Northeast China. Among them, the location of the closure of the Paleo-Asian Ocean is a key issue of great interest. The formation of the Paleo-Asian Ocean began in the Early Paleozoic and began to close in the Late Paleozoic by multiple stages of subduction and collision, eventually forming the CAOB (Liu et al. 2017).

Although the discovery of landmark rock samples such as ophiolites and radiolarian bedded cherts (Wang and Fan 1997; Li et al. 2012; Huang et al. 2016) has enabled the approximate location of the Solonker Suture Zone to be traced and thus clarifying the tectonic boundary of the paleo oceanic plate. However, the closure location of the Paleo-Asian Ocean remains a controversial issue due to the lack of constraints from deep physical models (Xiao et al. 2003; Eizenhöfer et al. 2014; Wilde 2015). Some scholars have suggested that the main basin of the Paleo-Asian Ocean finally closed from west to east in a temporal sequence along with a line form, and ended in NE China (Xiao et al. 2003; Liu et al. 2019); some scholars have also provided paleobiological evidence for the suture zone along the line of the Xar Moron River (Wang and Fan 1997).

Geophysical methods provides the scientific basis for an in-depth discussion of plate movements, tectonic processes, and their evolution patterns. Scholars have performed some comprehensive geophysical analyses of the eastern CAOB and nearby areas. Lu and Xia (1993) measured and interpreted a 960 km geological section from east-central Inner Mongolia to southern Liaoning by various methods, including seismic, geomagnetic, and heat flow, and revealed that the crust–mantle structure of the region is generally characterized by the vertical layers and horizontal blocks formation from the perspective of deep physical properties. For the lithospheric structure of the Xing'an Mongolia orogenic belt on the eastern CAOB, Xiong et al. (2015) conducted a comprehensive geophysical profiling study, such as the deep seismic reflection profile, the wide-angle refraction/reflection profile, and the magnetotelluric survey. In terms of the seismic inversion and interpretation, scholars have done much work, including the deep seismic reflection method

(Li et al. 2013; Hou et al. 2015), the receiver function method (Zhang et al. 2014a; Zhang et al. 2018), travel-time tomography method (Li et al. 2011), etc.

In terms of magnetotelluric (MT), Bai et al. (1993) and Bai and Zhang (1993) collected, processed, and interpreted data from 12 MT sites in the plate collision zones of eastern Inner Mongolia. Li et al. (2014) studied an MT profile about 500 km away from our study area, and obtained that the profile was divided into two region: low resistivity widely distributed in the northern part, and high resistance in the southern part. Liang et al. (2016) revealed the lithospheric structure of the Da Xing'an Mountains and the post-collisional extension record of the southern margin of the Central Asian orogenic belt through the study of deep electrical structures. Ye et al. (2019) identified the phases of electrical anomalies by anisotropic inversion methods, giving an essential constraint on the closure position of the Paleo-Asian Ocean. Mu et al. (2022) have proposed the relations between the high conductivity anomalies at crust–mantle scale in the eastern segment of the CAOB and the Paleo-Pacific Plate subduction with long-period MT data. All of the above studies have a common purpose, which is to provide the geophysical basis for the CAOB to determine the location of the Solonker Suture Zone by studying the subduction of the Paleo-Asian Oceanic crust. However, to the best knowledge, there is very little geophysical work in our study area, hence it is necessary to improve the research here.

The study area of this paper is located within the range from 116°24′ E to 122°11′ E and 42°44′ N to 45°65′ N, from Zhangwu County, Liaoning Province in the south to East-Ujimqin Banner, Inner Mongolia Autonomous Region in the north in China. The profile crosses several major areas from north to south, such as the Hegenshan Suture Zone, the Solonker Suture Zone, and the northern margin of the North China Craton. The present study area is close to NE China and is more susceptible to the modification effect of the Xing'an Mongolia orogenic belt after the Late Devonian. It is challenging to determine the location of the suture zone by surface geological studies, and the geophysical methods will provide some other interpretations. MT plays an essential role in revealing both the structure and physical state of the crust and upper mantle (Unsworth 2010). The study area of this paper has a unique geological background, where the both sides of the suture zone are basins. To be more specific, our study area is in between two Mesozoic–Cenozoic basins with a north–south direction. The south part is the southern margin of the Songliao Basin, and the north part is the southern margin of the Erlian Basin. The deeper parts beneath these two basins may have clear low-resistivity features that will facilitate the estimation of high-resistivity anomalies in the lithosphere, which is the evidence of the subduction of paleo-oceanic crust. At locations adjacent to the present study area, not so many MT data have been collected. To the best of our knowledge, there are only 12 MT sites have been set, and the inversion results have insufficient resolution (Bai et al. 1993; Bai and Zhang 1993). Specifically, within the range of more than 200 km, the resistivity model is only laterally divided into 5 regions. In the vertical direction, each region has a structure of 4–6 layers, but only the value range of resistivity is given for each layer. Therefore, it is vital to develop a more extensive and in-depth MT research for the eastern part of CAOB in the study area.

In this paper, we have provided a reliable deep resistivity model for studying the closure position of the Paleo-Asian Ocean near NE China and discussed some basis for analyzing the role of the Paleo-Pacific Plate subduction in the region. In addition, we will also further elaborate on the geological implications of the deep electrical structure by comparing the physical differences between the boundary areas of the massifs, such as Erguna Massif and Xing'an Massif, and their main parts.

Acquisition, processing, and analysis of MT data

Data acquisition

MT is a natural source electromagnetic method in the frequency domain that can determine the resistivity of the Earth by measuring the natural electromagnetic field on the surface (Rikitake 1950; Tikhonov 1950; Cagniard 1953). In this paper, the data set from 100 broadband MT stations was collected by Jilin University in 2018 from East-Ujimqin Banner, Inner Mongolia, to Zhangwu County, Liaoning Province. For each station, we used GPS synchronization. The average acquisition time was over 20 h. The MT profile is 500 km long with 5 km station spacing, holding an overall orientation of about NW 45°. Along with the profile, it passed through Haertao Town of Zhangwu County, Kulun Banner, Naiman Banner, Alukeerqin Banner, Lindong Town of Balinzuo Banner, Bayanhua Town and Gaorihan Town of West-Ujimqin Banner, Daotenaoer Town of East-Ujimqin Banner, etc. The locations of the MT sites are shown in Fig. 1. For field data acquisition, the Phoenix MTU-5 system was used. For each site, we measured two orthogonal horizontal electric field components (E_x, E_y) and three orthogonal magnetic field components (H_x, H_y, H_z) with subscripts x, y, and z representing north–south, east–west and vertical directions, respectively. After data processing, we obtain the information of impedance tensors. The MT profile was bent near Bayanhua Town for reasons, such as research objectives and the funding budget. One of our research objectives is to discuss the basin-range coupling characteristics of the study area, so it is

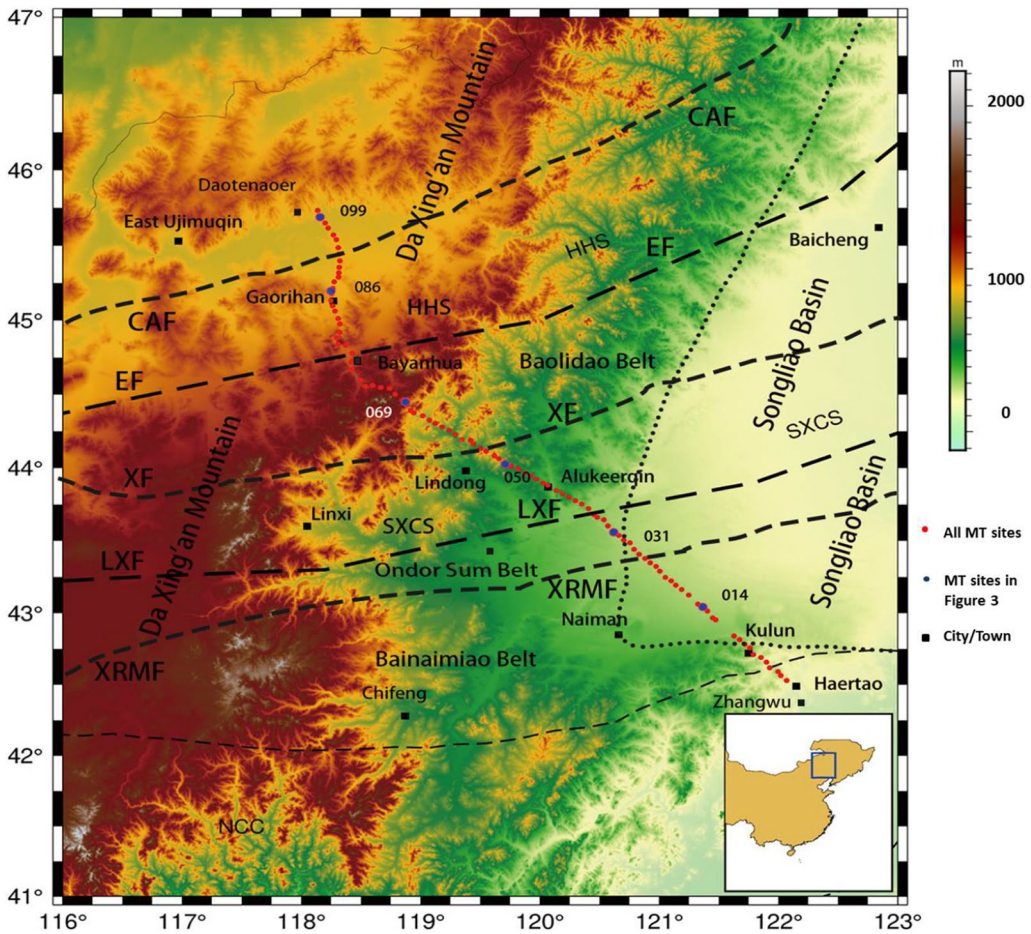

Fig. 1 Map of site locations. HHS represents the Hegenshan–Heihe Suture, and SXCS represents the Solonker-Xar Moron-Changchun Suture. In this paper, we use the Hegenshan Suture and Solonker Suture as abbreviations, respectively. NCC represents the North China Craton. CAF, EF, XF, LXF, and XRMF represent the Chagan Obo fault, the Erlian–Hegenshan Fault, the Xilinhot Fault, the Linxi Fault, and the Xar Moron River Fault, respectively

an efficient strategy to set more MT sites in the southern edge of the Erlian Basin by bending the profile. In addition, if we follow the direction of the southern part of the profile, we have to cross some mountainous areas without roads and private meadows. The paths of these areas are either very rugged or closed-to-traffic for environmental protection. Before the inversion and data processing, we will project the positions of each MT site to a straight line in advance.

Data processing

First, we use the SSMT2000 software to perform a fast Fourier transform on the original broadband MT time series to obtain data in the frequency domain. Then, after the process of robust regression and manual selection of power spectrums, the high-quality impedance tensor information is obtained. As shown in Fig. 2, the band of discrete sampling points is about 0.003-2000s. As shown by the apparent resistivity and phase curves of specific sites within each tectonic unit (blue dots in Fig. 1), they are significantly different for different tectonic units, and all have continuity except for the curves of Site 069 in middle and long-period bands. Sites 014 and 031 are located at the southern margin of the Songliao Basin, showing low-resistivity characteristics in the short-period band. Site 050 is located in the intersection area of the basin and Da Xing'an mountain, showing high-resistivity characteristics in the middle-period band. Site 069 is located near the Baiyinuoer mining area, with serious interference in the middle and long-period bands. Sites 086 and 099 are located in the pastoral areas of West-Ujimqin and East-Ujimqin Banner, respectively, with little interference from cultural noise. The static shift is the phenomenon of an overall parallel shift in the observed apparent resistivity curve due to small-scale near-surface resistivity inhomogeneities or topography(Jones 1988). Here, the correction of static shifts is considered in the process of inversion by allowing them to be free

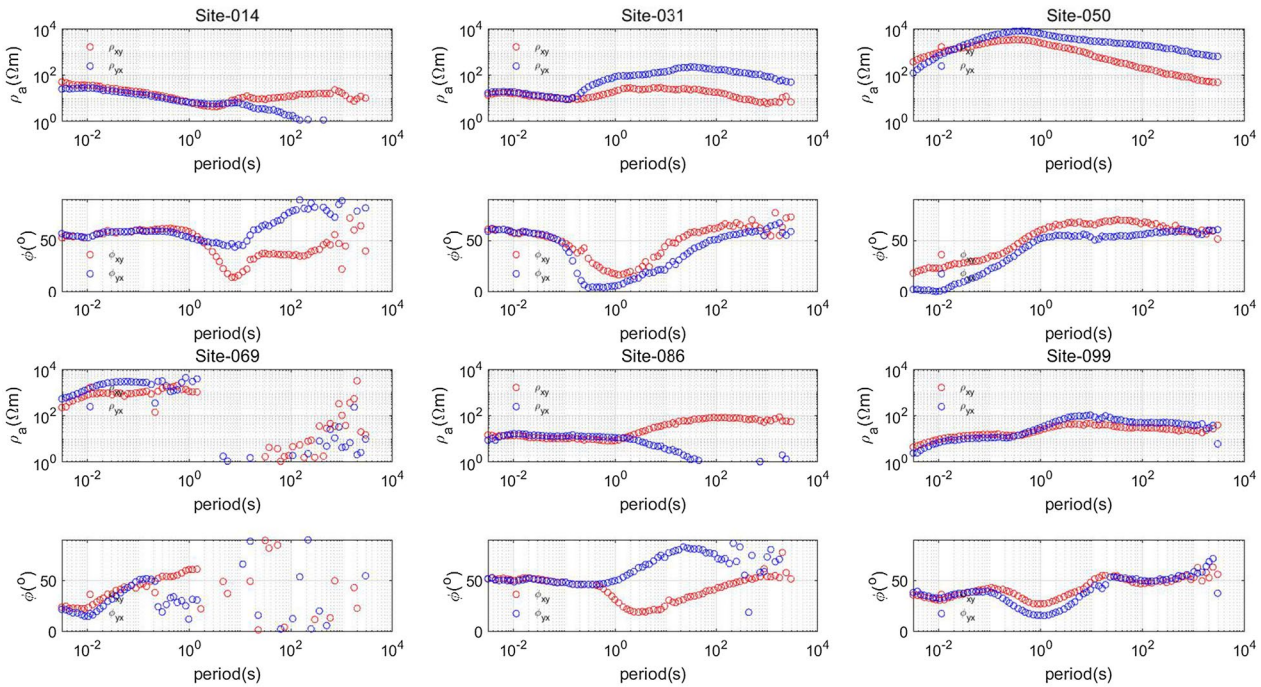

Fig. 2 Apparent resistivity (ρ_a) and phase (ϕ) curves for typical and original MT sites. The red and blue labels represent the apparent resistivity and phase from the elements of the impedance tensor matrix Z_{xy} and Z_{yx}, respectively

parameters(de Groot-Hedlin 1991). Therefore, a regularized inversion is applied to solve simultaneously for the resistivities and static shifts.

Dimensionality analysis

To obtain accurate inversion results, we first performed dimensionality analysis on the MT data and used it to determine the dimensionality of the subsurface model. Using Bahr (1991) decomposition and Groom–Bailey (GB) (1989) decomposition, we analyzed the data separately. Figure 3 shows the variation of the two-dimensional skew angle with period. When the two-dimensional deviation of most period bands is less than 0.3, the subsurface electrical structure can be approximated as a two-dimensional model; when the two-dimensional deviation is generally greater than 0.3, the model has a solid three-dimensional characteristic. Except for the long and medium period bands of the survey sites near the Baiyinuoer mine, the two-dimensional skew angle of most of the sites and frequencies bands in the study area is less than 0.3. It indicates that the profile has a prominent two-dimensional characteristic, and the subsurface electrical structure can be inverted and interpreted in two dimensions. For the cases above 0.3, it is mainly caused by multiple noises in the mine area. Before the inversion process, we will remove the data's long and medium period components in this region. For example, for site 069, we will keep only its short-period components.

In addition, the phase tensor analysis (Caldwell et al. 2004) is widely used to justify the feasibility of 2-D MT inversion. In a perfect 2-D MT model, the skew values are always zero. When most absolute skew values of the whole profile are low, such as 70% is less than 3, we can make the 2-D inversion and interpretation. The high skew values imply probable 3-D resistivity structures or distortions. If the value is more than 9, it can be removed from the inversion process. In Fig. 4, we provide the pseudo-section of absolute skew values in phase tensor analysis from our profile by the MTpy (Krieger and Peacock 2014; Kirkby et al. 2019). More than 70% of the skew values are less than 3, which is another favorable evidence for the 2-D MT inversion.

Geoelectric strike direction analysis

We analyzed the electrical principal axis directions of the data for all sites with all period points with GB decomposition (Groom and Bailey 1989) and found that the consistency is relatively poor. Therefore, dividing the MT profile into several sections and performing the principal axis analysis is reasonable. We divided the sites into three groups from south to north, roughly based on the Solonker Suture Zone and Hegenshan Suture Zone locations in Fig. 1. Figure 5a represents the rose diagram of

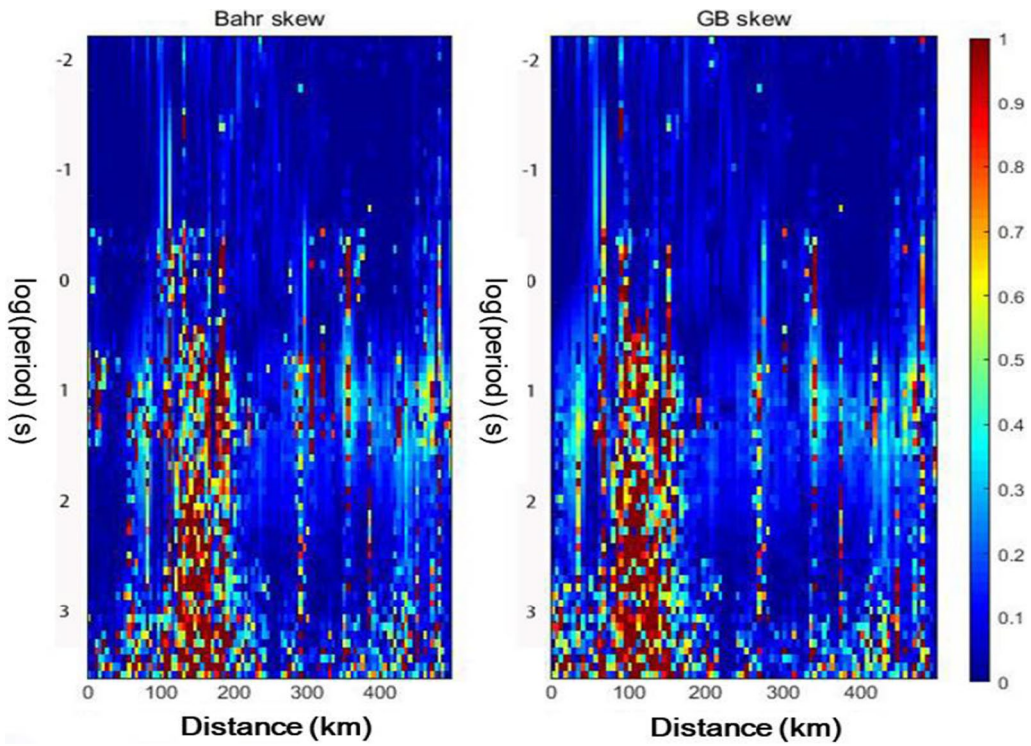

Fig. 3 Bahr and GB Skewness. The left side represents the north

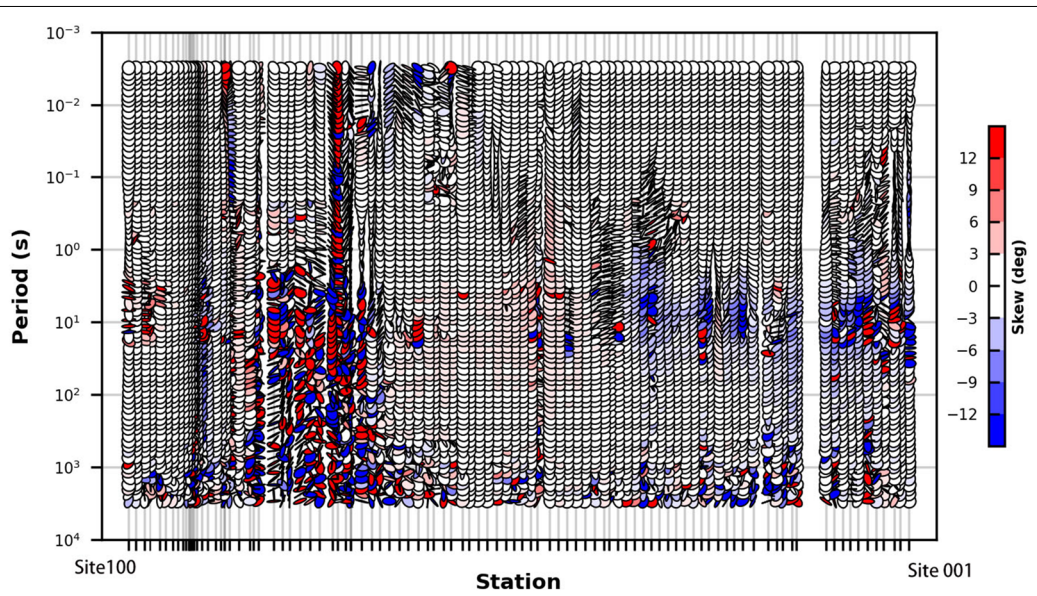

Fig. 4 Pseudo-section of phase tensors

sites 1 to 30, whose overall strike direction is about NE 60°; Fig. 5b represents the rose diagram of sites 31–70, whose overall strike direction is about NE 25°; Fig. 5c represents the rose diagram of sites 71–100, whose overall strike direction is about NE 45°. Since the regional tectonic strike is close to the northeast, and the field electric and magnetic data is collected in north–south, and east–west directions, the original apparent resistivity

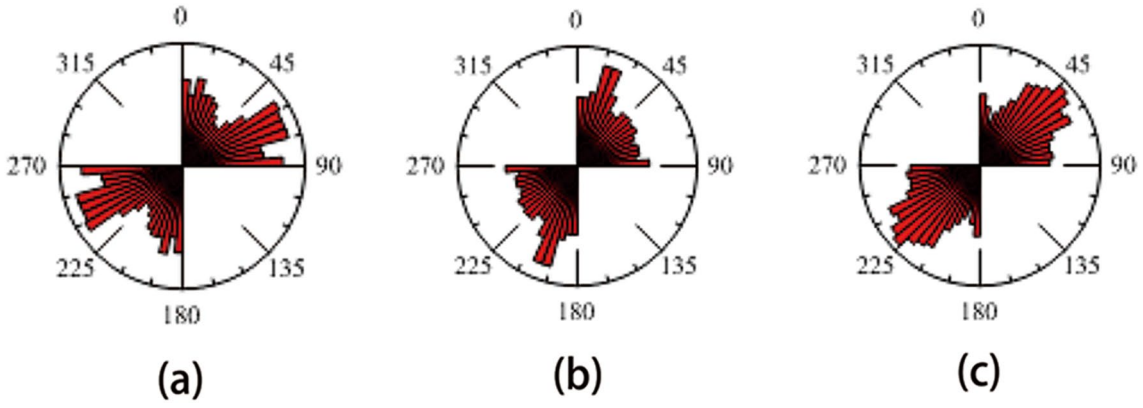

Fig. 5 Rose diagrams. **a**–**c** Typical principal axis rose diagrams for sites 1–30, 31–70, and 71–100, respectively

and phase curves can be rotated clockwise by 45°. Thus, the TE polarization pattern data parallel to the strike are obtained from the apparent resistivity ρ_{xy} and the impedance phase ϕ_{xy} and the TM polarization pattern data perpendicular to the strike are obtained from the apparent resistivity ρ_{yx} and the impedance phase ϕ_{yx}.

Inversion

The polarization patterns, TE and TM, are commonly used in MT inversion problems. The TM mode is related to the H-polarized wave, and the TE mode is related to the E-polarized wave. The inversion in the TM mode is not easily affected by the 3D inhomogeneities (Berdichevsky et al. 1998). In contrast, the response of the TE mode differs significantly from the actual 3D XY mode response in the long-period band. Indeed, the TM mode brings most of the structure information; however, the TE mode does not charge the structure, and its anomalies are related to its inductive nature (Berdichevsky et al. 1998; Chave and Jones 2012). Therefore, the following two approaches are usually used in the 2D MT inversion problems. One is to use the joint inversion of TE and TM modes with smaller weights for data of the TE mode in calculating the objective function values, and the other is to perform the inversion in the TM mode directly. This paper will adopt the first approach and apply the nonlinear conjugate gradient method (Rodi and Mackie 2001) for inversion in the TE and TM modes. The results of the joint inversion of TE and TM modes are more advantageous to show the real conditions of the subsurface model. Unfortunately, we have not collected the tipper data of all sites for the reason of lacking magnetic coils. Therefore, we only use the TE and TM data in the following inversion process.

The inversions were performed separately at different regularization factors τ. In Fig. 6, an L-curve was made with the model roughness as the horizontal axis (Oldenburg and Li 2005), and the root means square (RMS) error as the vertical axis. The L-curve criterion is an efficient way to choose the optimal regularization factors. The idea is based on the trade-off between regularization terms and fitting error terms. The value of τ located at the curve's inflection point corresponds to the inversion result with smaller fitting error and stronger model smoothness. When $\tau = 30$ is chosen, the fitting error is significantly higher; when $\tau = 5$ is chosen, the fitting error decreases by about 10%, while the roughness increases by nearly 50%. Therefore, the inversion results at $\tau = 10$ are chosen here as the final electrical model. For all inversions with different regularization factors, we set the grid profile to be 131 × 112. The horizontal step size is 5 km, and the vertical step size is increasing with depth from about 0.5–20 km. In addition, the initial model is a uniform

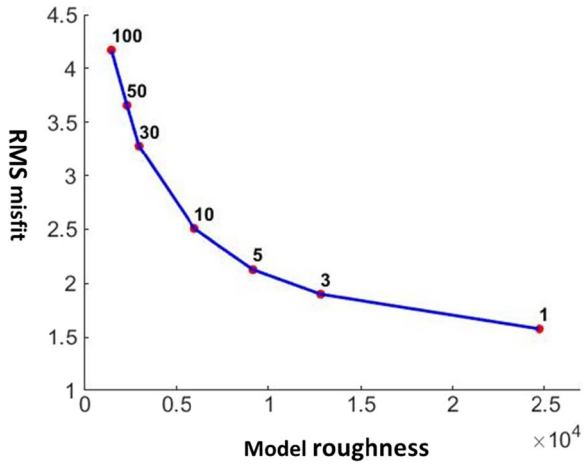

Fig. 6 L-curve between Model Roughness and RMS Misfits

half-space model of 100 Ωm, and the error thresholds for apparent resistivity and phase are 10% and 5% for the TM mode, and 30% and 5% for the TE mode. When the regularization factor is set to be 10, after 200 iterations, we obtain the final RMS misfit of 2.51. The final inversion results are shown in Fig. 7.

In Fig. 7, the vertical coordinates represent the depth, and the horizontal coordinates represent the accumulated distance of each survey site. To show the resistivity model more clearly, we set up the vertical scale to be 1.6 times of the horizontal scale. The colors such as red and yellow represent low resistivity, and blue represents high resistivity. C1, C2, C3, C4, C5, C6, and C7 are the low-resistivity bodies, and R1, R2, R3, R4, R5, and R6 are used to mark the high-resistivity bodies. As can be seen from the figure, the electrical model is tectonically complex. The profile from left to right can be roughly divided into three regions: north, central, and south. The Hegenshan Belt is the northern region, which contains Hegenshan Suture Zone; the Baolidao Belt, the Solonker Suture Zone, and the Ondor Sum Belt are the central region; the Bainimiao Belt is the southern region, which is located at the northern margin of the North China Craton. Here, the locations of the Hegenshan Belt and SSZ in Fig. 7 are relatively close to that of HHS and SXCS in Fig. 1. More precisely, the SXCS should include the SSZ and its surrounding area, while the SSZ is the specific suture location of the plates, which is identified in this paper.

In the northern part of the profile, C2 is a low-resistivity layer with an overall resistivity of less than 10 Ω m. In the deeper part, there is a high-resistivity body R1 and low-resistivity bodies C1 and C3 connected to C2. The southern side of the central region has a large-scale low-resistivity body C4 in the inner 10–30 km of the crust, with a high-resistivity body R5 below. Its northern side is composed of high-resistivity bodies R2, R3 and R4 collaged together. The low-resistivity body C7 in its central area is large in scale and connected to the low-resistivity body C4. In the southern region of the profile, the electrical model can be divided into three layers from shallow to deep. The first layer is the low-resistivity body C5 within the crust. The thickness is about 10–20 km, and the resistivity of less than 10 Ωm overall. The second layer is the high-resistivity body R6, with the thickness of about 40–80 km and the resistivity of more than 1000 Ωm. The third layer is the high conductivity layer C6 in the upper mantle, with the resistivity of less than 50 Ωm in general.

In Fig. 8, we provide the pseudo-sections of TM andTE modes. Obviously, the synthetic data and the measured data in TM mode are very close. In the TE mode, the resistivity data fitted very well. However, we only obtain the overall trend of the phase data in the TE mode, and does not fit the measure data well in some details. In general, the inversion results are valid for geological interpretation.

We have also made sensitivity tests for our inversion results. There are many ways to complete the sensitivity analysis in the MT inversion. Here, we choose different initial models as uniform half-space model of 10, 100 and 1000 Ωm, respectively. The paramters in the inversion are selected the same ones as before. Figure 9c shows the inversion result we introduced in Fig. 7. Indeed, most of the major anomlies in Fig. 9c are reflected in a and b. The main difference between them is only in the specific

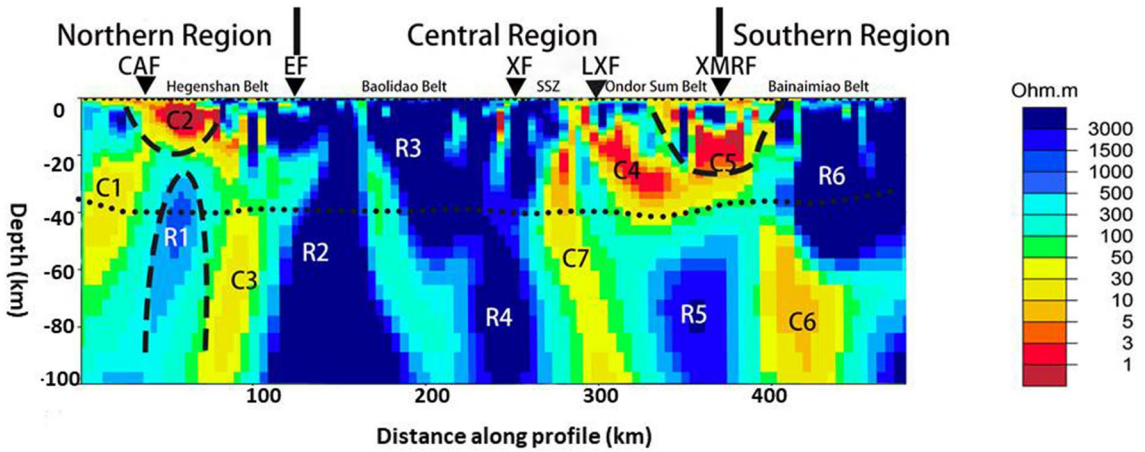

Fig. 7 Inversion results. The left side represents the north. Here, CAF indicates Chagan Obo Fault, EF indicates Erlian–Hegenshan Fault, XF indicates Xinlinhot Fault, SSZ indicates Solonker Suture Zone, LXF indicates Linxi Fault, and XMRF indicates Xar Moron River Fault. The dotted line around 40 km represents the Moho (Fu et al. 2021). C1 and C5 circled by dashed lines, represent the Meso-Cenozoic basins related to the Erlian Basin and the Songliao Basin

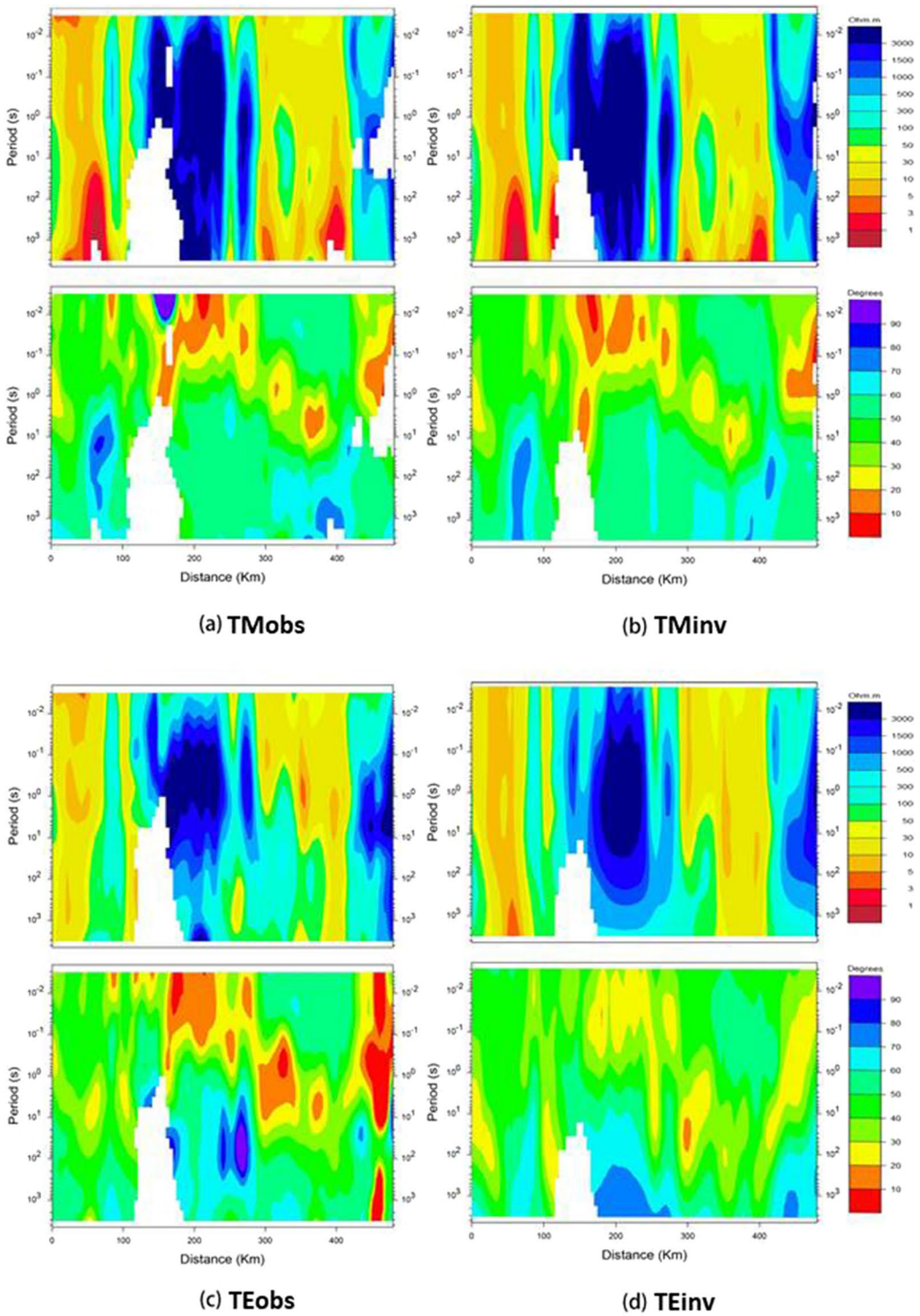

Fig. 8 Pseudo-sections of TM and TE modes. The left side represents the north. The subplots **a**–**d** are the pseudo-sections of measured data in TM mode, inversion response in TM mode, measured data in TE mode and inversion response in TE mode, respectively

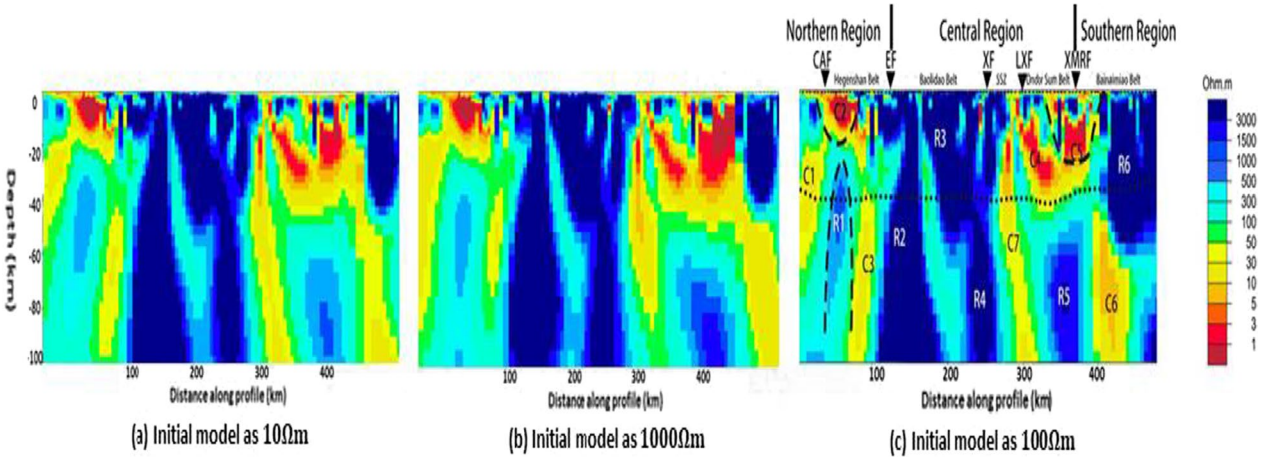

Fig. 9 Sensitivity tests. **a**–**c** Inversion results from initial resistivity modelsof 10, and 1000 and 100 Ωm

shape. Therefore, we believe that our inversion results are less sensitive to different intial models, and are provided with certain robustness.

Results and discussion

The northern part: the Hegenshan Belt

The northern part of the profile belongs to the Hegenshan Belt, adjacent to the southwest corner of the Erguna–Xing'an Massif in Northeast China. Some scholars have studied the deep electrical structure of the central part of the Erguna–Xing'an Massif. Liu et al. (2015) studied the electrical structure beneath the Hailar Basin and found that the upper and middle crust of the basin is generally divided into four layers of "low -high -low –high" resistivity, especially there are large-scale low-resistivity strips with significant thickness variations between 6 and 26 km. Liang et al. (2017) studied the electrical structure of the Erguna Massif, Xing'an Massif, and the collisional collage zone of the two massifs. They found that the low-resistivity body beneath the collision zone in their two dimensional MT profile is about 80 km in lateral direction, and over 100 km in vertical direction, but the middle and upper crust still contain obvious high-resistivity anomalies.

The middle and upper crust in this region is dominated by low-resistivity anomaly C2, which may be caused by the significant effect of crustal extension after the collision between massifs when the Hegenshan Ocean, a branch of the Paleo-Asian Ocean, was closed and formed the Hegenshan Suture. Some scholars have found that the geothermal heat flow value in the nearby area is significantly above the average value in North China (Zhang et al. 2020b), which also provides a basis for magmatic activity in the region. The high-resistivity body R1 in the lithospheric mantle has undergone continuous subductions, which has resulted in a continuous upwelling of mantle material since the Jurassic. Eventually, it has formed an overall low-resistivity feature in the middle and upper crust, which is also distinctly different from the main part of the Erguna–Xing'an Massif. The middle and lower crustal part of low-resistivity body C2 is connected to the Baiyinuoer mining area, presumed to be a basaltic magma rich in mineralized materials (Tong et al. 2010). Du and Lei (2019) discussed the relations between the upwelling materials and low-velocity anomalies generated by Pn arrivals around Erlian Basin.

The two low-resistivity bodies C1 and C3 at 20–70 km below the surface correspond to the Chagan Obo Fault and the Erlian–Hegenshan Fault, respectively, which may be channels to receive the mantle material. This region is a tectonic form of three primary low-resistivity bodies C1, C2, and C3, wrapping high-resistivity body R1. C1 and C3 have prominent dip characteristics following the deep physical evidence of southward subduction of the Mongolian–Okhotsk tectonic system since the Late Paleozoic. Though this area is far away from the Mongolia–Okhotsk Suture, the influence of the Mongol–Okhotsk tectonic system on the thermal upwelling of the Greater Xing'an Range can be proven by the geochemistry evidence (Zhang et al. 2020a). R1 might be a piece of delaminated lithosphere caused by the upwelling and southward subduction of the Paleo Asian Ocean (Fig. 10b–d), which we will discuss later.

The central area: the Baolidao Belt, the Solonker Suture Zone, and the Ondor Sum Belt

The central area of the profile, including the Baolidao Belt, the Solonker Suture Zone, and the Ondor Sum Belt, is adjacent to the Songnen Massif on its northeast

side. Liu et al. (2011) found a 50 km deep Nengjiang lithospheric fault in the collage zone between the Xing'an and Songnen massifs in the study of deep tectonics at the western boundary of the Songliao Basin. High-resistivity blocks dominate the Xing'an Massif in the western part of the fault in the crust. In contrast, the overall low-resistivity characterizes the Songnen Massif in the eastern part of a basin's crust. Like the main body of the Xing'an Massif, the Baolidao Belt also shows a highly resistive crust–mantle feature with a depth of more than 100 km, which indicates that this area is influenced by the Da Xing'an Mountains system significantly.

In particular, there are relatively low-resistivity blocks between the large-scale high-resistivity anomalies in this area, which mainly reflects that the eastern part of CAOB experienced multiple interplate subduction and collision during the formation process. The existence of supercrustal low-resistivity anomalies up to 50 km deep beneath the Solonker Suture Zone in this region might be due to the more intense bidirectional subduction of the lithospheric mantle on both sides, resulting in a larger scale of thermal material upwelling. The electrical structure of the Ondor Sum Belt in this region is the same as that of the main part of the Songnen Massif in the crustal range.

The high-resistivity bodies R2, R3, and R4 located below the Baolidao Belt may be mainly multi-phase granites, peridotites, and other igneous rocks, and metamorphic rocks, such as gneisses and hornblende. The material between R2 and R3 with the resistivity of about 100 Ωm, located in the middle and lower crust, should be a fracture zone containing water or other low-resistivity media, related to the filling of fluids in an extension environment during the late collisional period, and may have served as a channel for the upwelling of mineral-rich magma. The differences in the dip directions of the three large high-resistivity bodies also reflect that the CAOB has undergone multi-phase subduction, collision, and collage with different directions. The depth of R2 and R4 reaches the upper mantle, which may be related to the island arc collapse after the arc-continent collision in the middle Paleozoic (Li et al. 2017a, 2017b). It is also consistent with previous inferences that the lithosphere in the Da Xing'an Mountains region is thicker compared to the Songliao Basin.

Based on the distribution characteristics of the ophiolite (Huang et al. 2016), it has been hypothesized that the Hegenshan Suture Zone was the location of the closure of the Hegenshan Ocean in the early Late Paleozoic. The unidirectional accretion of the continental crust during this period was significant due to the collisional effect of the continental and oceanic crusts. However, by studying the state of Mg–Fe–super-Mg–Fe rocks, Shao et al. (2019) found that no obvious effects of subduction and collision occurred during the convergence of plates in the local area Hegenshan Suture Zone. However, some fragments of ancient continental crust were constantly collaged and embedded in the suture zone during the closure of the ocean basin. The high-resistivity body R2 is enormous in scale and shows vertical morphology, especially the northern side is more precipitous than the other. The reason may be due to the unidirectional accretion of the continental crust caused by collision on one hand, which ensures the vast scale of R2; on the other hand, in the collage effect of ancient continental crust after collisions, the originally slightly tilted high-resistivity body R2 after the collision was "compensated" by tiny continental crusts, and finally showed vertical and steep-standing morphology.

In the Mesozoic and Cenozoic periods, the orogenic system shifted from collision to intra-continental deformation (Fig. 10e), and a large amount of mantle-sourced material entered the crust under the action of the superposition of basin-range coupling and continental–crust accretion, which further intensified the continental–crust vertical accretion, and then formed Baiyinuoer and other mineral concentration areas. Therefore, the morphology of high-resistivity body R2 has not been fundamentally changed in this stage and still maintains the vertical morphology. The high-resistivity body R3 corresponds to the areas of the West Ujimqin Banner and the Alukeerqin Banner. Its large-scale feature may be attributed to the continental–crustal accretionary movements in eastern Inner Mongolia during the Early Paleozoic and Late Paleozoic periods.

The Ondor Sum Belt is located on the south side of the Solonker Suture Zone, a subduction zone formed adjacent to the North China Craton in the Early Paleozoic. There are middle and lower crustal low-resistivity body C4 and high-resistivity body R5 in the mantle. In general,

(See figure on next page.)

Fig. 10 Tectonic evolution scenarios. **a** Paleo-Asian Ocean northward subduction in early Paleozoic. The Southern Mongolia microplate and the North China Craton began to convergent. **b** Paleo-Asian Ocean began southward subduction in middle and late Paleozoic. The pattern of bidirectional subductions has been formed. **c** Continental collision in late Paleozoic and early Mesozoic. The Paleo-Asian Ocean has been closed in the Solonker Suture Zone. **d** Post-collisional extension in middle and late Mesozoic. A larger scale of thermal material was upwelling. Baiyinuoer and other mineral concentration areas began to form. **e** Intra-continental deformation from late Mesozoic to the present. The lithosphere has been thinned in the North China Craton. The subduction of Paleo-Pacific Plate began

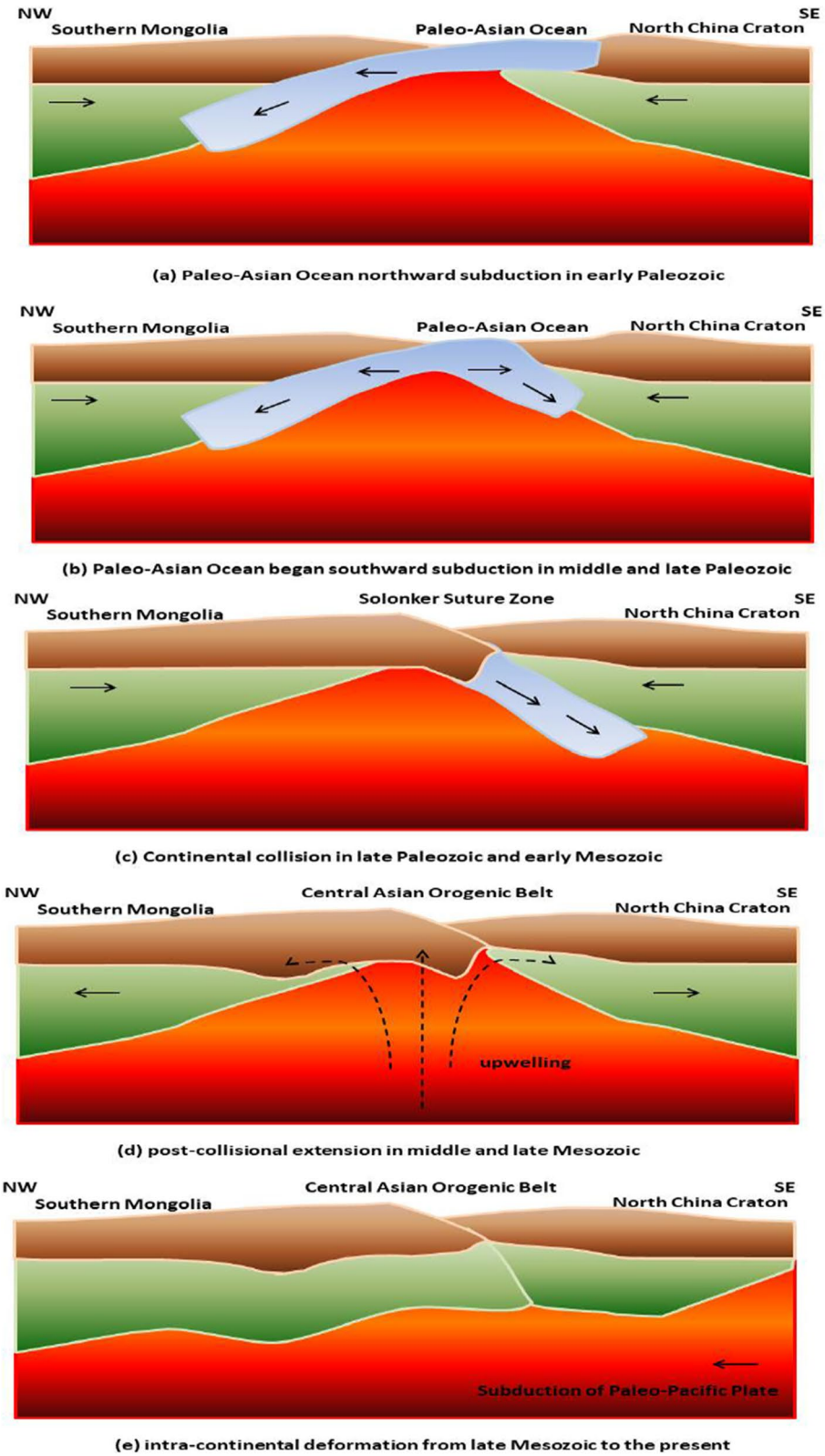

Fig. 10 (See legend on previous page.)

the low-resistivity bodies in the middle and lower crust are often inferred to be dominated by one of highly connected graphite or sulfur-bearing (carbon-bearing) sediments, partial melting material, brine-bearing fracture zones, etc. C4 should not be highly connected graphite, because larger scale graphite is not easily preserved stably. In addition, C4 is relatively weakly connected to the low-resistivity fault zone on both sides. C4 may be oceanic sedimentary rocks retained in the crust, because it is located at the southern boundary of the Solonker Suture Zone.

Through the study of metamorphic basalt volcanic rocks, Chu et al. (2013) provided evidence for the continuous occurrence of several extensional movements in the region since the Early Permian. Therefore, low-resistivity body C4 may be related to the upwelling of material from the upper mantle and may also be the result of sulfur- or carbon-bearing sediments left over from the southward subduction of high-resistivity body R5, but should not be the result of graphite (Yardley and Valley 1997) and the presence of water in the crust (Marquis and Hyndman, 1992). Since there are no clear magmatic chambers or vents beneath C4, we prefer C4 to be oceanic sediments, rather than upwelling materials.

Through geochemical and other studies, most scholars commonly agree that there was bidirectional north–south subduction during the closure of the Paleo-Asian Ocean. For example, by studying the geochemical characteristics of magmatic zircons and the spatial–temporal distribution of Permian granitic magmatism, Jing et al. (2021) concluded that the formation of Middle and Late Permian granites on the northern margin of the North China Craton was related to the southward subduction of the Paleo-Asian Ocean (Fig. 10b, c); by analyzing the ages of prograde biotite from paragneisses, Li et al. (2017a) found the onset of collision of accretionary wedges with continents during the northward subduction of the Paleo-Asian Ocean. They discussed that the process might have continued until 282 Ma. Furthermore, during the continuous northward subduction of the Paleo-Asian Ocean crust in Paleozoic (Fig. 10a), fragmental materials from the Southern Mongolian microplate and the Bolidao Belt were deposited in the forearc zone. At the same time, they did not originate from the North China Craton, which also suggests the existence of the Solonker Suture Zone in the CAOB, separating the northward subduction zone from the southward subduction zone.

However, because the surface rock samples have undergone many geological movements, the study of the deep physical parameters is still of great importance if we hope to infer the location of the suture zone more accurately. In our study area, the high-resistivity bodies R4 and R5 are lithospheric mantles with opposite dip directions located on both sides of the Solonker Suture Zone, in indicating the bidirectional subduction of the Paleo-Asian Ocean to the north and south, respectively (Ye et al. 2019). It supports the view that the CAOB is generated in a bidirectional subduction mode. The high-resistivity body R5 shows a southward trend, and its depth exceeds 100 km, which is evidence of the southward subduction of the Paleo-Asian oceanic crust with the lithosphere. In addition, the seismic tomography results indicates the southward subduction of the Paleo-Asian Ocean (Luan et al. 2022).

It is in agreement with the assumption that the oceanic crust beneath the Ondor Sum Belt was subducted to a depth of more than 100 km based on the relationship between the K_2O content of the rocks and the depth of subduction (Hu 1990). The high-resistivity body R4 shows a northward trend, evidence that the Paleo-Asian oceanic crust subducted northward with the lithospheric mantle (Fig. 10a, b). Therefore, R4 should be the mixture of ancient oceanic crust and lithospheric mantle. The Solonker Suture Zone is underlain by low-resistivity body C7, which reaches the upper mantle at depth and may have originated from the upwelling of hot material after the bidirectional subduction of the Palaeo-Asian Ocean.

Based on the MT research of Ye et al. (2019) from central Inner Mongolia, a few hundred kilometers away, the forward edge of a part of the highly resistive paleo-oceanic crust of the Paleo-Asian Ocean subducts southward beyond the Chifeng Fault. However, this paper's forward edge of the highly resistive paleo-oceanic crust R5 is only subducting as far as the Xar Moron River Fault, which is more than 100 km from the Chifeng Fault along with the profile. We suggest that this is, because the study area here is further east and more susceptible to subduction of the Paleo-Pacific Plate. The Paleo-Pacific Plate plunges to about 600-km deep in NE China (Zhao and Ohtani 2009). Moreover, the plate movement caused magma from the upper mantle to stagnate the continuously southward subducting paleo-oceanic crust and formed magma chambers within the upper mantle and crust, respectively. Thus, high-resistivity R4 and R5 can be used as a more reliable deep physical basis for the closure position of the Paleo-Asian Ocean.

In addition, it has been suggested that the Solonker Suture Zone divides the CAOB into two parts, the Northern Orogenic Belt and the Southern Orogenic Belt. Although we have not studied the part of the Northern Orogenic Belt outside China, we have found that low-resistivity bodies C4 and C2 correspond to two depression zones to the north and south of the eastern part of the CAOB, respectively, reflecting the regional tectonic characteristics of basin-range coupling from the perspective of electrical structure (Liang et al. 2016; Pang et al. 2020).

The southern area: the Bainaimiao Belt

The Bainaimiao Belt in the southern region of the profile lies to the south of the Xar Moron River Fault and is a part of the northern margin of the North China Craton. The low-resistivity body C5 in the crust probably formed during post-collisional extension (Fig. 10d), and the low-resistivity features are associated with mantle-derived materials. Its shallow material should be the Mesozoic and Cenozoic sedimentary layers.

Based on the relative positions and distribution patterns of the low-resistivity bodies, such as C4 and C6, we infer C6 as the partial melting materials, had been upwelling due to the lithospheric delamination and provided material sources for the low-resistivity bodies in the middle and lower crust on both sides of the fault. After cooling by the surrounding high-resistivity bodies R5 and R6, the resistivity of the transport channel between them is slightly higher. As a result, the lithospheric delamination effect is more pronounced in the northern region of the high-resistant body R6 due to its closer proximity to the magma channel between C4 and C6; the southern region retains more of the thickened part of the lithosphere due to its closer proximity to the central part of the old and cold craton. Chen et al. (2009) also obtained a similar results that the lithosphere is significantly thinned in the eastern NCC by the teleseismic S-receiver functions imaging.

A large and irregularly shaped high-resistivity body, R6, exists on the southern side of the Xar Moron River Fault, showing a trend of "shallow north and deep south". The upper and middle crust of the northern part of R6 may be a thrust nappe structure distributed from north to south. Based on the Rb–Sr and Ar–Ar isotopic ages, the early activity that gave rise to the structure can be traced back to 450–410 Ma (Zhou et al. 2018). The difference in dip angle between the northern block C4 and the southern block C5 and R6 of the Xar Moron River Fault is significant. Probably it is due to the fact that the northern margin of the North China Craton has undergone three main stages of continental subduction orogeny, intra-continental compression orogeny, and intra-continental extension orogeny, accompanied by approximately regular changes in the direction of the main stress field during different periods of the Phanerozoic (Wu 2000). During the early to mid-Mesozoic, the lithosphere of the northern margin of the North China Craton was still undergoing a violent thickening process. Subsequently, the thickening process was intensified by magma underplating with intra-continental compression orogeny. During the Mesozoic and Cenozoic, replacement and delamination following magma underplating led by intra-continental extension thinned the lithosphere at the northern margin of the North China Craton. In addition, during the Late Palaeozoic, the direction of maximum principal stress was dominated by a near NS orientation; during the Mesozoic, the direction of principal stress gradually shifted to an EW direction (Zhang et al. 2009). It helped, to some extent, to form the less regular geometry of R6.

There is some controversy over the upper mantle part of R6. Results from seismic deep reflection profiles suggest the presence of an intra-mantle reflection interface in the southern part of the Xar Moron River Fault, which might be an ancient crustal structure that has sunk into the mantle through delamination or paleo-oceanic crust in a remnant of the subduction zone (Zhang et al. 2014b). However, large-scale ophiolites have not been found for the present time in this region, which is far away from the well-known ophiolitic mixed rock belts, such as the Xar Moron River and the Daqing Ranch-Diyanmiao (Liu et al. 2019). Therefore, we suggest that the upper mantle part of the highly resistive body R6 should not be residual paleo-oceanic crust but mainly originate from continental crustal accretion under the tectonic regime of the northern margin of North China Craton.

Conclusions

An MT study was performed in the eastern CAOB near NE China, which is very important for understanding the tectonic evolution process in this region. Two large-scale high-resistivity bodies (R4 and R5) in the upper mantle, corresponding to the bidirectional subduction of the crust during the closure of the Paleo-Asian Ocean, provide a more critical and reliable basis for interpreting the closure location of the Solonker Suture Zone and give us a renewed insight into the genesis of the orogenic belt.

The large-scale electrical anomalies in the north and south generally show a northward and southward dip, respectively, reflecting the closure of the Paleo-Asian Ocean. The subduction of the paleo-oceanic plate brought about the upwelling of mantle material, making the study area as a whole characterized by basin-range coupling.

The large-scale high-resistivity bodies with different dip directions beneath the Baolidao Belt show that the study area has experienced several subductions and collisions during its formation at an inter-plate zone. However, the vertical and steep northern flank of the high-resistivity body R2, close to the Hegenshan Belt, reflects the post-collisional "compensation" of tiny continental crusts.

Abbreviations

CAOB: Central Asian Orogenic Belt; MT: Magnetotelluric; TE: Transverse electric; TM: Transverse magnetic; GB decomposition: Groom–Bailey decomposition; 2D: Two-dimensional; 3D: Three-dimensional; RMS: Root mean square.

Acknowledgements
The authors would like to express their deep respect and sincere gratitude to two anonymous reviewers. The authors are especially grateful to Prof. Baojun Yang for his devoted direction. Thanks to Prof. Tonglin Li for his suggestions. We thank Prof. Jiangtao Han's team for their selfless help in many aspects. We thank the members of our research group in solid geophysics for their hard field work. Thanks to the developers of the MTpy software for MT data processing.

Author contributions
All authors were involved with this work. PZ was involved in most of the data acquisition, inversion, and interpretation and was responsible for writing the paper. CL was the leader of all the authors' research groups and was responsible for all aspects of the project collaboration. YL was involved in the whole process of data acquisition and was the leader of the MT project. YT is a seismologist and gave many shining suggestions on the geological understanding and interpretation of the study area. XC was involved in the geological interpretation and the discussion of the MT principles. YC is a Ph.D. student and was responsible for the work related to the pre-processing of the data. All authors read and approved the final manuscript.

Authors' information
The second author CL is the Executive Director of the Chinese Geophysical Society. The corresponding author YL is the member of the First Standing Committee of the Youth Working Committee of the Chinese Geophysical Society.

Funding
The research is supported by the National Key Research and Development Program Topics (2017YFC0601301, 2018YFC0603701, 2016YFC0600505, 2021YFC1523401); special fund of Key Laboratory of Geo-Exploration Instruments, Ministry of Education; Jilin University High-level Science and Technology Innovation Team Construction Project (2017TD-14).

Availability of data and materials
The MT data collected for our study are archived and can be accessed by contacting Jilin University.

Declarations

Ethics approval and consent to participate
Not applicable.

Consent for publication
Not applicable.

Competing interests
The authors declare that they have no competing interests.

Author details
[1]College of Geo-Exploration Science and Technology, Jilin University, Changchun 130026, China. [2]Central Lab of Applied Geophysics, Changchun 130026, China.

Received: 14 September 2021 Accepted: 23 September 2022
Published online: 13 October 2022

References

Bahr K (1991) Geological noise in magnetotelluric data: a classification of distortion types. Phys Earth Planet Inter 66:24–38
Bai DH, Zhang L (1993) A magnetotelluric study of the Paleozoic collision zone in the east of Inner Mongolia——II: two dimensional modelling. Chin J Geophys 36:773–783
Bai DH, Zhang L, Kong XR (1993) A magnetotelluric study of the Paleozoic collision zone in the east of Inner Mongolia——I: observations and data analyses. Chin J Geophys 36:326–336
Berdichevsky MN, Dmitriev VI, Pozdnjakova EE (1998) On two-dimensional interpretation of magnetotelluric soundings. Geophys J Int 133(3):585–606
Cagniard L (1953) Basic theory of the magneto-telluric method of geophysical prospecting. Geophysics 18(3):605–635
Caldwell TG, Bibby HM, Brown C (2004) The magnetotelluric phase tensor. Geophys J Int 158(2):457–469
Chave A, Jones A (2012) The magnetotelluric method: theory and practice. Cambridge University Press, New York
Chen L, Cheng C, Wei Z (2009) Seismic evidence for significant lateral variations in lithospheric thickness beneath the central and western North China Craton. Earth Planet Sci Lett 286(1–2):171–183
Chu H, Zhang J, Wei C, Wang H, Ren Y (2013) A new interpretation of the tectonic setting and age of meta-basic volcanics in the Ondor Sum Group, Inner Mongolia. Chin Sci Bull 58:3580–3587
de Groot-Hedlin C (1991) Removal of static shift in two dimensions by regularized inversion. Geophysics 56(12):2102–2106
Du M, Lei J (2019) Pn anisotropic tomography of Northeast China and its implications to mantle dynamics. J Asian Earth Sci 171:334–347
Eizenhöfer P, Zhao G, Zhang J, Sun M (2014) Final closure of the Paleo-Asian Ocean along the Solonker suture zone: constraints from geochronological and geochemical data of Permian volcanic and sedimentary rocks. Tectonics 33:441–463
Fu W, Hou H, Gao R, Zhou J, Zhang X, Guo L, Pan Z (2021) Lithospheric structures of the central Solonker-Xar Moron-Changchun-Yanji Suture (Inner Mongolia) revealed by a deep seismic reflection profile. Tectonophysics 817:229043
Groom R, Bailey R (1989) Decomposition of magnetotelluric impedance tensors in the presence of local three-dimensional galvanic distortion. J Geophys Res Solid Earth 94(B2):1913–1925
Hou H, Wang H, Gao R, Li Q, Li H, Xiong X, Tong Y (2015) Fine crustal structure and deformation beneath the Great Xing'an Ranges, CAOB: revealed by deep seismic reflection profile. J Asian Earth Sci 113:491–500
Hu X (1990) Evolution of the early Paleozoic continental margin in the margin of North China Craton. Peking University Press, Beijing
Huang B, Fu D, Li S, Ge M, Zhou W (2016) The age and tectonic implications of the Hegenshan ophiolite in Inner Mongolia. Acta Petrologica Sinica 32:158–176
Jing Y, Ji Z, Ge W, Dong Y, Yang H, Bi J (2021) Middle–late permian I-type granitoids from the Diaobingshan region in the northern margin of the North China Craton: insight into southward subduction of the Paleo-Asian Ocean. Int Geol Rev 63:357–379
Jones AG (1988) Static shift of magnetotelluric data and its removal in a sedimentary basin environment. Geophysics 53(7):967–978
Kirkby AL, Zhang F, Peacock J, Hassan R, Duan J (2019) The MTPy software package for magnetotelluric data analysis and visualisation. J Open Source Softw 4(37):1358
Krieger L, Peacock J (2014) MTpy: a Python toolbox for magnetotellurics. Comput Geosci 72:167–175
Li Z, Hao T, Xu Y (2011) Uppermost mantle structure of the North China Craton: constraints from interstation Pn travel time difference tomography. Chin Sci Bull 56:1691
Li Y, Wang J, Li H, Dong P, Liu Y, Liu D, Bai H (2012) Recognition of Diyanmiao ophiolite in Xi U jimqin Banner, Inner Mongolia. Acta Petrologica Sinica 28(4):1282–1290
Li W, Keller G, Gao R, Li Q, Cox C, Hou H, Zhang S (2013) Crustal structure of the northern margin of the North China Craton and adjacent region from SinoProbe02 North China seismic WAR/R experiment. Tectonophysics 606:116–126
Li B, Wei WB, Zhang LT (2014) Electrical structure revealed by magnetotelluric data at the east part of central Asian orogenic belt, central Inner Mongolia. Appl Mech Mater 448:3788–3791
Li Y, Brouwer F, Xiao W, Zheng J (2017a) A Paleozoic fore-arc complex in the eastern Central Asian Orogenic Belt: Petrology, geochemistry and zircon U-Pb-Hf isotopic composition of paragneisses from the Xilingol Complex in Inner Mongolia, China. Gondwana Res 47:323–341
Li Y, Brouwer F, Xiao W, Zheng J (2017b) Late Devonian to early Carboniferous arc-related magmatism in the Baolidao arc, Inner Mongolia, China: Significance for southward accretion of the eastern Central Asian orogenic belt. CSA Bull 129:677–697

Liang H, Gao R, Hou H, Jin S, Liu G (2016) Deep electrical structure beneath the Da Hinggan Ling and the junction zone with adjacent basins and their tectonic relationship at a lithospheric scale. Chin J Geophys 59:1696–1704
Liang H, Jin S, Wei W, Gao R, Liu G (2017) Deep electrical structure of the eastern margin of the Erguna massif and the western margin of the Xing'an massif. Chin J Geophys 60:564–574
Liu C, Yang B, Wang Z, Wang D, Feng X, Lu Q, Liu Y (2011) The deep structure of the western boundary belt of the Songliao basin: the geoelectric evidence. Chin J Geophys 54:401–406
Liu Z, Ye G, Wei W, Jin S (2015) Study of the central-upper crust electrical structure of Hailar Basin. Chin J Geophys 58:4425–4435
Liu Y, Li W, Feng Z et al (2017) A review of the Paleozoic tectonics in the eastern part of Central Asian Orogenic Belt. Gondwana Res 43:123–148
Liu Y, Feng Z, Jiang L, Jin W, Liang C (2019) Ophiolite in the eastern Central Asian Orogenic Belt, NE China. Acta Petrologica Sinica 35:3017–3047
Lu Z, Xia H (1993) Transect from Dong Ujimqinqi, Nei Mongol, to Donggou, Liaoning. Chin J Geophys 36:765–772
Luan JP, Tang J, Xu WL et al (2022) Accretion kinematics and driving mechanism of the eastern Central Asian Orogenic Belt: Insights from seismic tomography and middle Permian-Middle Triassic magmatism in central Jilin Province. Gondwana Res 101:114–131
Marquis G, Hyndman R (1992) Geophysical support for aqueous fluids in the deep crust: seismic and electrical relationships. Geophys J Int 110:91–105
Mu Q, Han J, Hou H et al (2022) Effect of the Western Pacific plate subduction on upper mantle in the eastern segment of the Central Asian Orogenic Belt: revealed by long-period magnetotelluric data. Tectonophysics 837:229436
Oldenburg D W, Li Y (2005) Inversion for applied geophysics: a tutorial. Near-Surface Geophysics, p 89–150
Pang Y, Guo X, Zhang X et al (2020) Late Mesozoic and Cenozoic tectonothermal history and geodynamic implications of the Great Xing'an Range, NE China. J Asian Earth Sci 189:104155
Rodi W, Mackie R (2001) Nonlinear conjugate gradients algorithm for 2-D magnetotelluric inversion. Geophysics 66:174–187
Rikitake T (1950) The electrical state of the earth's interior as inferred from variations in earth's magnetic field. Bull Earthq Res Inst Tokyo Univ 28:45–219
Shao J (1991) Crustal evolution in the middle part of the northern margin of the Sino Korean plate. Peking University Press, Beijing
Shao J, Zhang L, Zhou X, Zhang L, Tang K (2019) A further study on the ophiolite in Hegenshan, Inner Mongolia. Acta Petrologica Sinica 35:2864–2872
Tang K, Wang Y, He G, Shao J (1995) Continental-margin structure of northeast china and its adjacent areas. Acta Geol Sin 3:241–258
Tikhonov AN (1950) On determining electrical characteristics of the deep layers of the Earth's crust//Doklady. Citeseer 73(2):295–297
Tong Y, Hong D, Wang T, Shi X, Zhang J, Zeng T (2010) Spatial and temporal distribution of granitoids in the middle segment of the Sino-Mongolian border and its tectonic and metallogenic implications. Acta Geoscientica Sinica 31:395–412
Unsworth M (2010) Magnetotelluric studies of active continent–continent collisions. Surv Geophys 31(2):137–161
Wang Y, Fan Z (1997) Discovery of Permian radiolarians in ophiolite belt on northern side of Xar Moron River, Nei Monggol and its geological significance. Acta Palaeontologica Sinica 36:58–69
Wang YN, Xu WL, Wang F et al (2018) New insights on the early Mesozoic evolution of multiple tectonic regimes in the northeastern North China Craton from the detrital zircon provenance of sedimentary strata. Solid Earth 9(6):1375–1397
Wilde S (2015) Final amalgamation of the Central Asian Orogenic Belt in NE China: Paleo-Asian Ocean closure versus Paleo-Pacific Plate subduction—a review of the evidence. Tectonophysics 662:345–362
Wu Z (2000) Three different types of Phanerozoic orogenesis of northern border area of North China Craton. J Geomech 6:46–53
Xiao W, Windley B, Hao J, Zhai M (2003) Accretion leading to collision and the Permian Solonker suture, Inner Mongolia, China: termination of the central Asian orogenic belt. Tectonics 22:1069–1088
Xiong X, Gao R, Li Y, Hou H, Liang H, Li W, Lu Z (2015) The lithosphere structure of the Great Xing'an Range in the eastern Central Asian Orogenic Belt: constrains from the joint geophysical profiling. J Asian Earth Sci 113:481–490
Yardley B, Valley J (1997) The petrologic case for a dry lower crust. J Geophys Res Solid Earth 102:12173–12185
Ye G, Unsworth M, Wei W, Jin S, Liu Z (2019) The lithospheric structure of the Solonker suture zone and adjacent areas: crustal anisotropy revealed by a high-resolution magnetotelluric study. J Geophys Res Solid Earth 124:1142–1163
Zhang L, Wu H, Wan B, Chen Z (2009) Ages and geodynamic settings of Xilamulun Mo–Cu metallogenic belt in the northern part of the North China Craton. Gondwana Res 16:243–254
Zhang R, Wu Q, Sun L, He J, Gao Z (2014a) Crustal and lithospheric structure of Northeast China from S-wave receiver functions. Earth Planet Sci Lett 401:196–205
Zhang S, Gao R, Li H, Hou H, Wu H, Li Q, Liu M (2014b) Crustal structures revealed from a deep seismic reflection profile across the Solonker suture zone of the Central Asian Orogenic Belt, northern China: an integrated interpretation. Tectonophysics 612:26–39
Zhang H, Li Q, Ye Z, Gong C, Wang X (2018) New seismic evidence for continental collision during the assembly of the central Asian orogenic belt. J Geophys Res Solid Earth 123:6687–6702
Zhang C, Quan JY, Zhang YJ et al (2020a) Late Mesozoic tectonic evolution of the southern Great Xing'an Range, NE China: evidence from whole-rock geochemistry, and zircon UPb ages and Hf isotopes from volcanic rocks. Lithos 362:105409
Zhang J, Huang S, Zuo Y, Zhou Y, Liu Z, Duan W, Wei X (2020b) Terrestrial heat flow in the baiyinchagan sag, erlian Basin, northern China. Geothermics 86:101799
Zhao D, Ohtani E (2009) Deep slab subduction and dehydration and their geodynamic consequences: evidence from seismology and mineral physics. Gondwana Res 16:401–413
Zhou Z, Zhang D, Gu Y, Wang G, Li H, Yu Y, Liu C, Liu W (2018) Characteristics of Bainaimiao thrust belt along Central Inner Mongolia in North China and its geological significance. Geotecton Metallog 42:1–17

Publisher's Note